An Inkjet-Printed Nonlinear-Element-Based Graph Neural Network for Solubility Prediction

Shahrin Akter, Syed Kamrul Islam, and Mohammad Rafiqul Haider
Dept. of Electrical Engineering and Computer Science
University of Missouri
Columbia, MO, U.S.A.
{shahrin.akter, islams, mhaider}@missouri.edu

***Abstract*—Inkjet printing is an emerging fabrication technique for flexible electronics, offering a simple fabrication method, environmental sustainability, and cost-effectiveness. Recent advancements in inkjet printing method have explored the implementation of computational devices such as transistors and relays using inkjet printing technology. Following this trend, a novel nonlinear computation device has been developed via inkjet printing, exhibiting I–V characteristics with nonlinearity analogous to activation functions commonly used in neural networks. In neural network, the activation function is used to introduce nonlinearity in neural networks and enables the network to learn the complex pattern of the dataset. To evaluate the performance of this device as an activation function, the mathematical model derived from its I–V curve was implemented within a graph neural network to predict the solubility of organic molecules. The neural network incorporating the nonlinear computation device demonstrated comparable performance to commonly used activation functions, including tanh and sigmoid, achieving mean squared error, root mean square error and R^2 score of 1.556, 1.247 and 0.62 respectively.**

***Index Terms*—Activation Function, Inkjet Printing Technology, Graph Neural Network, Solubility.**

I. Introduction

The concept of flexible electronics is gaining attention in both sensing and computational device applications due to their stretchable and conformable nature, allowing these devices to adapt to the shape of organic objects [1]. Among the various fabrication techniques available for flexible electronics, inkjet printing technology has emerged as one of the most widely adopted fabrication methods [2]. This popularity stems from its advantages over other fabrication approaches, such as thin-film deposition [3], laser printing [4], and roll-to-roll processing. Specifically, inkjet printing offers benefits including low cost, a simplified fabrication process, environmental sustainability, and compatibility with low-power devices [5]. Furthermore, the versatility of inkjet printing enables the deposition of multiple nanoparticle inks on a variety of substrates, facilitating the design and development of a wide range of devices and exploring different characteristics of nanoparticle inks for device formation [6]–[8].

In alignment with these advancements, numerous inkjet-printed sensors have been successfully developed for diverse applications, including breathing flow monitoring [10] and pressure gradient mapping [11]. While these sensors are cost-effective and require minimal processing, their performance often remains inferior to that of solid-state sensors. To overcome these limitations and enhance the reliability and scalability of inkjet-printed sensors, artificial intelligence has been integrated into sensor operation [12], [13]. Motivated by these requirements, researchers have sought to implement various computational devices using inkjet printing technology. Furthermore, the fabrication of inkjet-printed computational devices such as transistors, memristors, and relays has been extensively investigated in the literature [14]–[16]. Prior state-of-the-art studies have demonstrated the development of inkjet-printed memristive device for neuromorphic computing, with mathematical modeling indicating its capability to form grid-like architectures for mapping data into higher dimensions and classifying image data [17] with simple machine learning model. In [18], S. D. Gardner *et al.* reported the fabrication of a fully inkjet-printed artificial neuron capable of implementing the hyperbolic sine activation function within neural networks. However, these devices typically operate within relatively high voltage ranges, which constrains their applicability in low-power circuit implementations.

In this study, a low-voltage flexible non-linear computing element is designed and fabricated using inkjet printing technology. This device exhibits nonlinearity comparable to that utilized in neural network activation functions such as hyperbolic tangent (*tanh*) in a very low operating voltage range of -0.5 V to +0.5 V. To investigate its potential as an activation function within neural networks, this nonlinear computation element has previously been applied successfully in echo state networks for Mackey-Glass time series data prediction [9] and in multilayer perceptrons for Fashion MNIST image classification tasks [19]. In this work, the device is integrated within a graph neural network framework with graph-type dataset to predict the solubility of various organic molecules, and its performance is evaluated against commonly used activation functions such as *tanh* and *sigmoid*.

The paper is organized in the following structure. Section II introduces the inkjet-printed nonlinear element, describing its fabrication process, electrical characterization, and mathematical modeling. Section III presents the graph neural network framework and the dataset utilized in this study. The experimental results are detailed and discussed in Section IV, followed by concluding remarks in Section V.

II. Inkjet Printed Nonlinear Computation Element

Inkjet printing has emerged as a promising fabrication technique for flexible electronics. In this study, a nonlinear element device was fabricated using an inkjet printing process. The device architecture, along with the relevant dimensions, is illustrated in Fig. 1(a). The device consists of centrally located floating square islands and triangular islands positioned on either side, with dimensions of 1.5 mm, and separated by 0.5 mm distance. Additionally, eight padframes, each measuring 5 mm and separated by $\theta = 45^\circ$ angle from each other, were incorporated into the design to facilitate electrical connections.

A. Fabrication Process

Inkjet printing technology offers a straightforward and versatile fabrication process. The fundamental steps of inkjet printing-based fabrication include designing the desired pattern using a 2D vector graphic tool, printing the pattern onto a substrate with an inkjet system, and curing the jetted ink pattern. Depending on specific research requirements, additional steps such as ink preprocessing, substrate surface preparation to enhance ink adhesion, and post-processing of the printed patterns may also be incorporated. The fabrication method employed in this study is outlined in the flowchart presented in Fig. 1(c). The device pattern was designed using Microsoft Publisher, and printing was performed using a modified Epson XP 960 inkjet printer adapted for silver nanoparticle ink deposition. In the first step, a $2.35\mu m$ thick layer of silver nanoparticle ink was printed onto a polyethylene terephthalate (PET) film substrate using the modified printer. This printed layer was subsequently cured on a hotplate at $90^\circ F$ for 4–5 minutes to prepare the device for the deposition of the second layer. The second layer, consisting of hexagonal boron nitride (hBN), was applied using a drop casting method. HBn is chosen as the second layer for device because it increases the charge density in the active region of the device. Two layers of hBN were deposited and cured with a hot air gun at $90^\circ F$ for 2–3 minutes. This results in a hBN layer with the thickness range of $2.35\mu m - 1.53\mu m$. In case of hBN layer, thickness varies in this wide range due to its spread over the substrate and silver layer. Finally, manual cuts were made in the open spaces between the islands to complete the device structure.

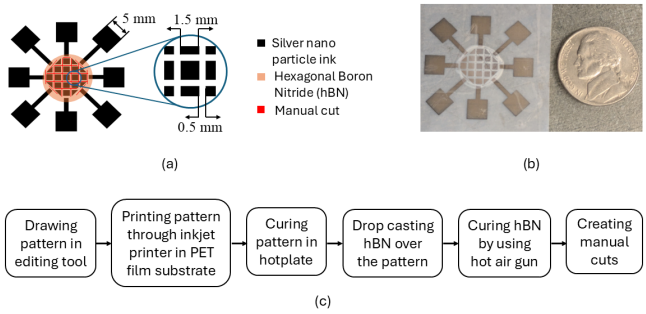

Fig. 1. (a) Inkjet printed nonlinear element device architecture along with the device dimension and material information, (b) a comparable image of the device with a dime, and (c) the device fabrication process flowchart.

B. Electrical Characterization

For the electrical characterization of the device, a Keithley 2604B Dual Channel Source Measure Unit was utilized. Voltage sweeps were performed across the device from -5 V to +5 V, followed by a reverse sweep from +5 V to -5 V, to generate a complete hysteresis loop. This procedure was repeated twice to evaluate the repeatability of the IV characteristics, and multiple trials with multiple sampled devices were conducted to further confirm the consistency of the measurements. In each test,the device shows repetitive I-V curve with its distinctive behavior. Additionally, I-V characteristics were measured across different padframe angles, revealing that with increasing padframe angles, the I-V curves exhibit an upward tilt, as shown in Fig. 2(b). Fig. 2(a) presents the I-V characteristics measured between two padframes oriented at an angle of 90°, where it is evident that the device begins to exhibit nonlinearity within a low voltage range of approximately -1 V to +1 V. During the forward voltage sweep, three distinct pinch-off points were observed near -1 V, -0.09 V, and +1.3 V, while in the reverse sweep, two pinch-off points were noted during the transition period. These pinch-off features were consistently observed across all measurement cycles and are attributed to charge trapping within the hexagonal boron nitride (hBN) layer. Importantly, the device demonstrates pronounced nonlinearity within a narrow voltage range of approximately -0.5 V to +0.5 V, indicating its potential suitability for low-power device applications.

C. Mathematical Modeling

The reverse path of the device's IV characteristics exhibits a profile similar to the hyperbolic tangent (tanh) function, which is widely utilized as an activation function in neural networks. This resemblance suggests the potential for employing the device's IV curve directly as an activation function within neural network architectures. To enable this, the forward and reverse paths of the IV curve are mathematically expressed using the following equations 1 and 2.

As the reverse path closely mimics the traditional tanh function, its curve-fitting formulation incorporates a modified tanh function with tunable coefficients and constants to control its slope and position, enabling accurate fitting to the measured reverse path. Similarly, the forward path demonstrates characteristics resembling a flipped sigmoid function. Therefore, the forward path is expressed using Equation 2. In addition, Gaussian functions are employed to replicate the pinch-off behavior observed in the IV curve.

$$f_{\text{reverse}}(x) = t(x) \times g_1(x) \times g_2(x) \tag{1}$$

$$f_{\text{forward}}(x) = s(x) \times g_3(x) \times g_4(x) \times g_5(x) \tag{2}$$

Here, *t(x)* and *s(x)* represent the modified *tanh* and sigmoid functions, respectively, while $g_1(x)$, $g_2(x)$, $g_3(x)$, $g_4(x)$, and $g_5(x)$ denote Gaussian functions used to model the pinch-off phenomena within the IV curves.

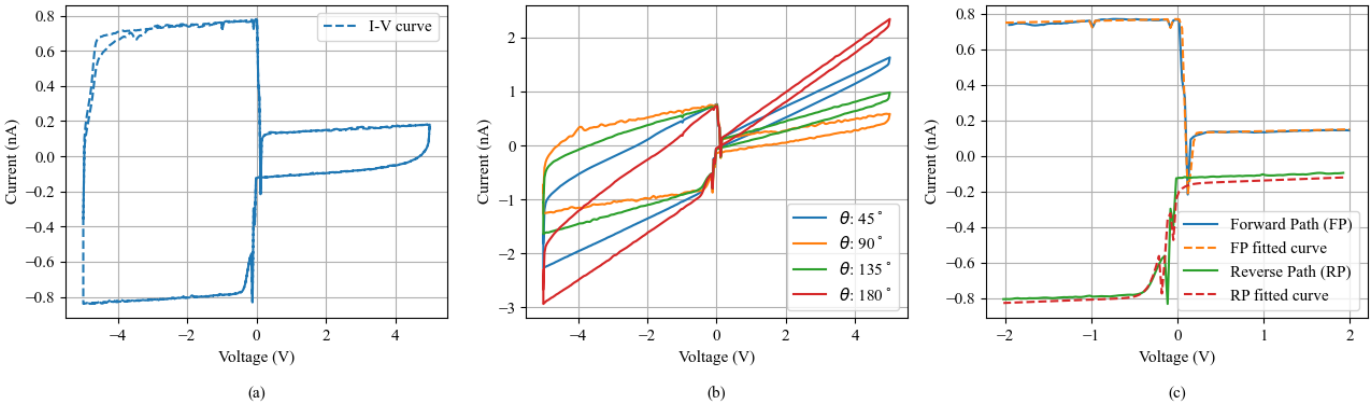

Fig. 2. (a) Two dual sweep I-V characteristics for nonlinear computation element show the repeatability of electrical characterization; (b) I-V characteristics of the nonlinear computation element measured at different padframe angles (θ). An increase in the angle between padframes results in an upward tilt in the I-V curves; (c) Forward and reverse paths of the I–V characteristics alongside their respective fitted equations, demonstrating the close agreement between experimental data and the fitted models.

The modified tanh and sigmoid functions are defined as follows:

$$t(x) = a\tanh(bx + c) + dx + e \tag{3}$$

$$s(x) = \left(\frac{t}{1 + e^{p(x-q)}} + rx\right) \tag{4}$$

The Gaussian functions used to replicate the pinch-off behavior are defined by:

$$g_n(x) = h_n \exp\left(-\frac{(x - \mu_n)^2}{2\sigma_n^2}\right) + m_n \tag{5}$$

where, $n = \{1, 2, 3, 4, 5\}$

In these formulations, the constants a, b, c, d, and e are used to adjust the slope and position of the *tanh* function to align with the experimental reverse path of IV data. Similarly, the constants p, q, r, and t control the slope and position of the sigmoid function for precise fitting in the forward path. In the Gaussian functions, the mean μ determines the position of the pinch-off, while the variance σ controls its width. The parameters h and m regulate the height and vertical position of the Gaussian functions, enabling accurate replication of the pinch-off behavior observed in the device's IV characteristics. The forward and reverse path of the IV curve is shown along with their respective fitted curves in Fig. 2(c).

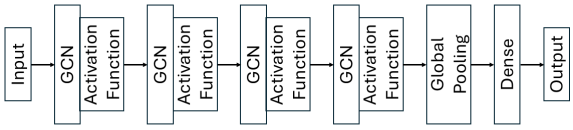

Fig. 3. Graph neural network model architecture.

III. Graph Neural Network

The IV curve of the nonlinear element exhibits a non-linearity comparable to activation functions commonly used in neural networks. To assess the potential of this nonlinear device as an activation function, the fitted equations of its IV characteristics are implemented within a graph neural network (GNN) framework to predict molecular solubility.

A. Dataset

For the regression task in the graph neural network, the MoleculeNet ESOL dataset is utilized [20]. This dataset serves as a benchmark for molecular property prediction and comprises 1,128 samples. Each sample includes the water solubility (log solubility in mol/L) along with the chemical structure of an organic compound, encoded as a SMILES string. The dataset is partitioned into training, validation, and testing subsets using an 8:1:1 ratio.

B. Model Description

GNNs are a class of deep neural networks designed to operate on graph-structured data and were first introduced by S. Franco et al. in 2008 [21]. Given the non-Euclidean structure of molecular data, GNNs are particularly effective for molecular datasets, motivating their selection as the machine learning model in this study. The basic architecture of the developed graph neural network is illustrated in Fig. 3.

The proposed model consists of four graph convolutional network (GCN) layers, each followed by an activation function. In this study, three different activation functions are evaluated: the traditional tanh, the sigmoid function, and the reverse path of the IV curve of the nonlinear device, which is named mTanh due to its behavior similar to that of the tanh function. Following the final GCN and activation function layer, a global pooling layer is applied, which is then followed by a linear dense layer serving as the output layer for regression tasks. For model training, mean squared error is utilized as the loss function, and the Adam optimizer is

employed for optimization. The model is trained using 80% of the dataset over 2000 epochs.

IV. Results

For the regression performance comparison of the nonlinear computation element with commonly used activation functions such as tanh and sigmoid, three evaluation metrics are employed: mean squared error (MSE), root mean squared error (RMSE) and coefficient of determination (R^2). These metrics are computed using Equations 6, 7 and 8.

$$\text{MSE} = \frac{1}{n}\sum_{i=1}^{n}(y_i - \hat{y}_i)^2 \tag{6}$$

$$\text{RMSE} = \sqrt{\frac{1}{n}\sum_{i=1}^{n}(y_i - \hat{y}_i)^2} \tag{7}$$

$$R^2 = 1 - \frac{\sum_{i=1}^{n}(y_i - \hat{y}i)^2}{\sum i = 1^n (y_i - \bar{y})^2} \tag{8}$$

Here, n, y_i, and $\hat{y}_i$ denote the total number of samples, the true values, and the predicted values from the model, respectively. An optimal regression performance is indicated by MSE and RMSE value approaching zero and R^2 value approaching one.

TABLE I
Regression performance comparison of nonlinear computation element with other activation functions in graph neural network.

Activation Function	MSE	RMSE	R^2 Score
Sigmoid	1.305	1.143	0.681
Tanh	0.898	0.947	0.781
mTanh	1.556	1.247	0.62

Fig. 4 and table I presents the comparative performance analysis of the different activation functions. From that table, it is evident that for tanh activation function, MSE and RMSE both are closest to zero, comparative to sigmoid and mTanh function. On the contrary for tanh, GNN model gives R^2 value closest to one compare to other two activation functions. The figure illustrates the scatter plots of the actual versus predicted solubility for each activation function along with the MSE, RMSE and the R^2 square in the label. The data points along the slope show the perfect prediction of solubility. Among the evaluated functions, the tanh activation yields the most concentrated scatter distribution, whereas the nonlinear computation element exhibits a more dispersed scatter pattern. This further confirms that the developed nonlinear computation element can function as an activation mechanism within a graph neural network. Although its performance does not surpass that of the tanh and sigmoid functions, the results demonstrate the feasibility of utilizing the nonlinear computation element as an activation function in machine learning models.

This nonlinear computational element does not surpass other activation functions in performance due to the occurrence of pinch-offs in the transition region, which can introduce instability in the learning process of neural network models. These pinch-offs primarily arise from charge trapping within defect states of the device. Appropriate surface treatments, such as plasma oxidation, can mitigate these issues by reducing defect density and trapped charge concentration. Furthermore, replacing the hBN dielectric layer with an alternative material exhibiting lower polarization could help minimize dips and overshoots in the device's I–V characteristics. As part of future work, efforts will focus on exploring alternative nanoparticle inks to achieve improved device morphology, as well as incorporating additional fabrication steps to enhance overall performance. Additionally, this device will be employed in the fabrication of an inkjet-printed echo state reservoir.

V. Conclusion

In this work, a flexible device was developed using inkjet printing technology, demonstrating I–V characteristics with nonlinearity analogous to activation functions commonly employed in neural networks. To evaluate its applicability as an activation function, the forward and reverse paths of the I–V curve were mathematically modeled, with the equation derived from the reverse path implemented as an activation function within a graph neural network to predict the solubility of various organic molecules. The performance of this nonlinear device was subsequently compared with widely used activation functions such as tanh and sigmoid. Although the device did not outperform these traditional activation functions, it exhibited comparable results, demonstrating its feasibility for use as an activation function in neural network models. This study highlights the potential of the developed device for future implementation in neuromorphic computing and neural network applications within flexible electronics utilizing inkjet printing technology.

Acknowledgment

This work was supported by the USA National Science Foundation (NSF) under Grant No. ECCS-2430440. Any opinions, findings, conclusions, or recommendations expressed in this material are those of the author(s) and do not necessarily reflect the views of the National Science Foundation.

References

[1] D. Corzo, G. Tostado-Blázquez, Guillermo and D. Baran, "Flexible electronics: status, challenges and opportunities," *Journal of Low Power Electronics and Applications*, vol. 1, pp. 594003, 2020.

[2] M. A. Shah, D. Lee, B. Lee and S. Hur, "Classifications and applications of inkjet printing technology: a review," *Journal of Low Power Electronics and Applications*, vol. 9, pp. 140079-140102, 2021.

[3] L. Maiolo, A. Pecora, F. Maita, A. Minotti, E. Zampetti, S. Pantalei, A. Macagnano, A. Bearzotti, D. Ricci and G. Fortunato, "Flexible sensing systems based on polysilicon thin film transistors technology," *Sensors and Actuators B: Chemical*, vol. 179, pp. 114-124, 2013.

[4] T. Han, A. Nag, N. Afsarimanesh, S. C. Mukhopadhyay, S. Kundu and Y. Xu, Yongzhao, "Laser-assisted printed flexible sensors: a review," *Sensors*, vol. 19, no. 6, pp. 1462, 2019.

[5] M. Singh, H. M. Haverinen, P. Dhagat and G. E. Jabbour, "Inkjet printing—process and its applications," *Advanced materials*, vol. 22, no. 6, pp. 673-685, 2010.

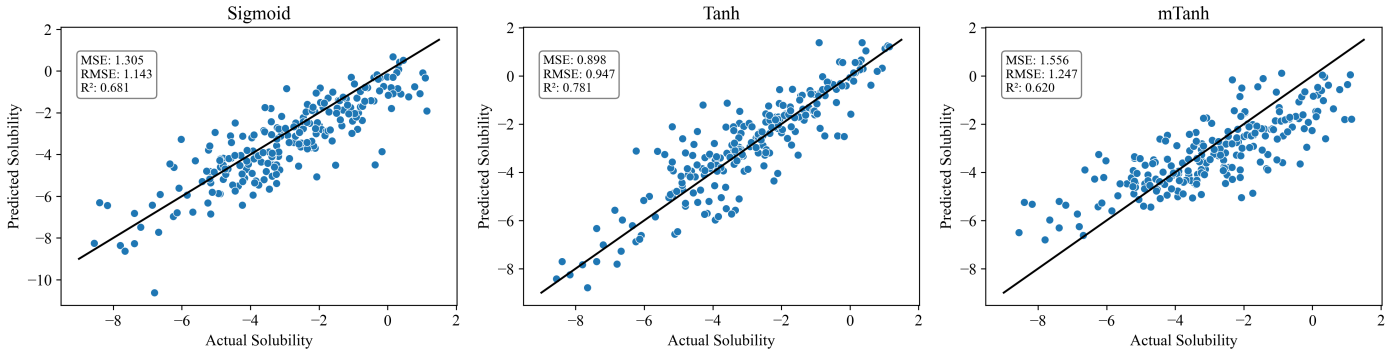

Fig. 4. Scatter plot of actual versus predicted solubility values for GNN models with different activation functions along with performance matrices. Data points lying along the diagonal indicate perfect predictions. The tanh function shows a higher concentration of points around the diagonal, suggesting better predictive performance, whereas the custom nonlinear computation element (mTanh) exhibits a more dispersed pattern, indicating relatively higher prediction error.

[6] S. D. Gardner, J. I. D. Alexander, Y. Massoud and M. R. Haider, "An inkjet-printed paper-based flexible sensor for pressure mapping applications," 2020 IEEE International Symposium on Circuits and Systems (ISCAS), Sevilla, Spain.

[7] S. D. Gardner, J. I. D. Alexander, Y. Massoud and M. R. Haider, "Aluminum-doped zinc oxide (zno) inkjet-printed piezoelectric array for pressure gradient mapping," 2019 IEEE 62nd International Midwest Symposium on Circuits and Systems (MWSCAS), Dallas, TX, USA.

[8] S. D. Gardner, J. I. D. Alexander, Y. Massoud and M. R. Haider, "An inkjet-printed capacitive sensor for ultra-low-power proximity and vibration detection," 2023 IEEE Wireless and Microwave Technology Conference (WAMICON), Melbourne, FL, USA.

[9] S. Akter and M. R. Haider, "A Low-Cost Minimally-Processed Inkjet-Printed Nonlinear Element for Reservoir Computing," 2024 IEEE Computer Society Annual Symposium on VLSI (ISVLSI), Knoxvile, TN, USA.

[10] R. Lu, M. R. Haider, S. D. Gardner, J. I. D. Alexander and Y. Massoud, "A paper-based inkjet-printed graphene sensor for breathing-flow monitoring," *IEEE Sensors Letters*, vol. 3, no. 2, pp. 1-4, 2018.

[11] S. D. Gardner, M. R. Haider, M. T. Islam, J. I. D. Alexander and Y. Massoud, "Aluminum-doped zinc oxide (zno) inkjet-printed piezoelectric array for pressure gradient mapping," 2019 IEEE 62nd International Midwest Symposium on Circuits and Systems (MWSCAS), Dallas, TX, USA.

[12] S. Akter and M. R. Haider, "Impact Localization in Inkjet-Printed Tactile Grid Sensor with Echo State Network," 2024 IEEE 67th International Midwest Symposium on Circuits and Systems (MWSCAS), Springfield, MA, USA.

[13] S. D. Gardner,A. Porbanderwala and M. R. Haider, "An Affordable Inkjet-Printed Foot Sole Sensor and Machine Learning for Telehealth Devices," *IEEE Sensors Letters*, vol. 7, no. 6, pp. 1-4, 2023.

[14] S. Chung, K. Cho, Kyungjune and T. Lee, "An inkjet-printed artificial neuron for physical reservoir computing," *Advanced science*, vol. 6, no. 6, pp. 1801445, 2019.

[15] H. Hu, A. Scholz, Y. Liu, Y. Tang, G. C. Marques and J. Aghassi-Hagmann, "A fully inkjet-printed unipolar metal oxide memristor for nonvolatile memory in printed electronics," *IEEE Transactions on Electron Devices*, vol. 70, no. 6, pp. 3051-3056, 2023.

[16] E. S. Park, Y. Chen, T. J. K. Liu and V. Subramanian, "A new switching device for printed electronics: inkjet-printed microelectromechanical relay," *Nano letters*, vol. 13, no. 11, pp. 5355-5360, 2013.

[17] T. Z. Adry, S. D. Gardner, S. Eliza and M. R. Haider, "Inkjet-Printed Memristor Device for Neuromorphic Computing: Fabrication, Modeling, and Reservoir Implementation," *International Journal of High Speed Electronics and Systems*, pp. 2640021, 2025.

[18] S. D. Gardner and M. R. Haider, "An inkjet-printed artificial neuron for physical reservoir computing," *IEEE Journal on Flexible Electronics*, vol. 1, no. 3, pp. 185-193, 2022.

[19] S. Akter and M. R. Haider, "mTanh: A Low-Cost Inkjet-Printed Vanishing Gradient Tolerant Activation Function," *Journal of Low Power Electronics and Applications*, vol. 15, no. 2, pp. 27, 2025.

[20] Z. Wu, B. Ramsundar, E. N. Feinberg, J. Gomes, C. Geniesse, A. S. Pappu, K. Leswing and V. Pande, "MoleculeNet: A Benchmark for Molecular Machine Learning," *Chemical Science*, vol. 9, no. 2, pp. 513–530, 2018.

[21] F. Scarselli, M. Gori, A. C. Tsoi, M. Hagenbuchner and G. Monfardini, "The graph neural network model," *IEEE transactions on neural networks*, vol. 20, no. 1, pp. 61–80, 2008.